Geomechanics and Engineering, *Vol. 25, No. 2 (2021) 159-170*
DOI: https://doi.org/10.12989/gae.2021.25.2.159

On the effect of void ratio and particle breakage on saturated hydraulic conductivity of tailing materials

Changkun Ma[1,2a], Chao Zhang*[1], Qinglin Chen[3], Zhenkai Pan[1] and Lei Ma[1]

[1]*State Key Laboratory of Geomechanics and Geotechnical Engineering, Institute of Rock and Soil Mechanics, Chinese Academy of Sciences, Wuhan, China*
[2]*University of Chinese Academy of Sciences, Beijing, China*
[3]*Jiangxi University of Science and Technology, Ganzhou, Jiangxi, China*

(Received January 11, 2021, Revised March 29, 2021, Accepted April 7, 2021)

Abstract. Particle size of tailings in different areas of dams varies due to sedimentation and separation. Saturated hydraulic conductivity of high-stacked talings materials are seriously affected by void ratio and particle breakage. Conjoined consolidation permeability tests were carried out using a self-developed high-stress permeability and consolidation apparatus. The hydraulic conductivity decreases nonlinearly with the increase of consolidation pressure. The seepage pattern of coarse-particle tailings is channel flow, and the seepage pattern of fine-particle tailings is scattered flow. The change rate of hydraulic conductivity of tailings with different particle sizes under high consolidation pressure tends to be identical. A hydraulic conductivity hysteresis is found in coarse-particle tailings. The hydraulic conductivity hysteresis is more obvious when the water head is lower. A new hydraulic conductivity-void ratio equation was derived by introducing the concept of effective void ratio and breakage index. The equation integrated the hydraulic conductivity equation with different particle sizes over a wide range of consolidation pressures.

Keywords: tailings; effective void ratio; particle breakage; hydraulic conductivity

1. Introduction

Tailings are the beneficiation remnants that contain low target components and not suitable for further separation. There are differences in the particle shape and particle gradation of tailings prepared under different mineral processing procedures. More and more fine particles accumulate in tailings dams with the increase in demand for mineral products and improved beneficiation technology. The number of tailings dams is limited due to national policy and environmental protection, so the existing tailings dams will be higher. Fine-particle and high-stacked dams are popular in the future. The study on the effect of void ratio and particle breakage on saturated hydraulic conductivity of tailing materials is necessary.

Fine-particle tailings have poor permeability and strong water holding capacity, which makes it difficult to dam such tailings (Horpibulsuk *et al.* 2011). Some papers have adopted new damming techniques such as the flocculants method, geofabriform method or reinforcement method to enhance the stability of the dams in order to overcome the challenges of fine-particle dams (Courtney *et al.* 2017, Robert 2000, Kim *et al.* 2019, Wang *et al.* 2020). Hydraulic conductivity is one of the most important and valuable parameters in studying fine-particle dams (Tavenas *et al.* 1983). Many researches have shown that hydraulic conductivity depends on a long list of parameters, such as porosity, clay content, fluid type, pore pressure and pore geometry (Lambe and Whitman 1969, Hilfer 1991, Bernabé 2010, Jang *et al.* 2011). These parameters are all discussed to make our research more comprehensive. In spite of the complexity, numerous researchers have suggested expressions for the hydraulic conductivity of soils (Kozeny 1927, Carman 1937, Taylor 1948, Mesri and Olson 1971, Samarasinghe *et al.* 1982). The applicability of these expressions to tailings (artificial sand) is worth discussing. The relationship between hydraulic conductivity and void ratio based on sandy soil is not suitable for clayey soil due to electrochemical reactions (such as the K-C equation). Taylor (1948) showed the inapplicability of fine-particle soil of such relations for due to the surface properties of the particles and the presence of ineffective pores. Many hydraulic conductivity-void ratio expressions also have been proposed for fine-particle soil. Ineffective pores mainly affect hydraulic conductivity from three aspects: geometric characteristics of pores and particles, the salinity of flow, and cation exchange capacity of minerals. Sedimentary separation by particle size occurs when the tailings slurry flows on the dry beach, and a fine-particle interlayer "lens" can be formed (Gomes *et al.* 2017). In this paper, the concept of effective void ratio and breakage index are introduced to propose a prediction of hydraulic conductivity in tailing dams.

Fig. 1 shows a diagram of a tailings deposition. The tailings at the bottom are subject to a large and increasing

*Corresponding author, Professor
E-mail: 20172001004@cqu.edu.cn
[a]Ph.D.
E-mail: machangkun16@mails.ucas.ac.cn

ISSN: 2005-307X (Print), 2092-6219 (Online)

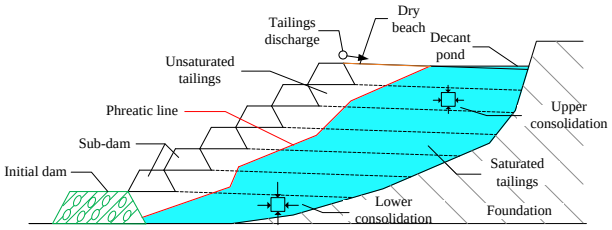

Fig. 1 Profile of tailings deposition

consolidation pressure as the dam height increases (James *et al*. 2011). For high-stacked tailings, the bottom stress can reach 4.4 MPa (take the dam height of 200 m and the average weight of 22 kN/m^3 as an example). The bottom tailings should be subject to a high consolidation pressure. The tailings particle breakage under high pressure can not be negligible. Our previous work studied the mechanical properties of tailings under high pressure within a confining pressure of 5 MPa (Zhang *et al.* 2020), which showed that the breakage of tailings particles under high pressure is not negligible. An experimental study on the hydraulic conductivity of tailings with different particle sizes under high consolidation pressure is conducted by the self-developed "High-stress Permeability and Consolidation Apparatus". The concept of breakage index and effective void ratio are introduced to modify the hydraulic conductivity equation and provide a theoretical basis for the construction of high tailing dams.

The aim of this paper is to study the water film and mineral composition of particles with different particle sizes because the particle size is one of the factors that affect hydraulic conductivity. The gradation curves after high-pressure consolidation are analyzed because the gradation curves are essential parameters for the breakage index. The qualitative and quantitative analyses of hydraulic conductivity under the effect of particle size and high consolidation pressure were carried out. Finally, the effective void ratio and breakage index are introduced to predict of hydraulic conductivity of tailings.

2. Materials and methods

2.1 Materials

Tailings materials used in the tests were acquired from the No. 4 dam of Dexing Copper Mine of Jiangxi Copper Group, China. The tailings dam is currently the largest tailings dam in Asia, with a design height of 208 m, and is a typical high-stacked tailings dam. It is almost impossible to obtain an undisturbed sample from the bottom of such a high tailing dam. Therefore, the remodeled tailings samples with different particle sizes were employed to study the compression and consolidation behavior of tailings under high pressure. The remodeled samples collected on site are dried in an oven (at 105°C) for 24 hours and passed through the target sieves. The D_{max} of the target sieves is 2 mm, 0.2 mm, 0.075 mm and 0.035 mm respectively. The four samples are marked as S20, S02, S_75, S_35 respectively. The tailings with an upper particle size limit of 0.035 mm are separated by an air classifier. The particles are separated into two piles by the fan of the air classifier. The frequency of the fan was adjusted with the laser particle size analyzer to reach the target particle size limit value. The gradation curves of the four tailings are discussed in detail in the Section 2.2, and physical properties of the four tailings samples are shown in Table 1. The four tailing samples are classified as sandy tailings, silty tailings, silty-clayey tailings, clayey tailings respectively (ASTM, 2017). The D_{max} of sample S20 is selected as 2 mm because the particle size of the original tailings sample does not exceed 2 mm, and the D_{max} of sample S_75 is selected as 0.075 mm because 0.075 mm is the critical value for fine and coarse particles. The other two values are inserted so that the four tailings samples belong to four different stickiness types.

Table 1 Physical properties of samples

Sample	S20	S02	S_75	S_35
Specific gravity *Gs*	2.87	2.85	2.82	2.78
Dry density ρ_d (g/cm^3)	1.6			
Initial void ratio e_0	0.794	0.781	0.763	0.738
Initial specific volume v	0.625			
Liquid limit ω_l (%)			28.8	40.4
Plastic limit ω_p (%)			16.9	20.1
Plastic index I_p			11.9	20.3
d_{10} (mm)	0.02	0.009	0.006	0.003
d_{30} (mm)	0.093	0.035	0.013	0.008
d_{50} (mm)	0.141	0.076	0.023	0.011
d_{60} (mm)	0.173	0.091	0.035	0.013
d_{90} (mm)	0.370	0.166	0.067	0.028
C_u*	7.5	10.1	5.8	4.3
C_c**	2.2	1.5	0.8	1.6
%Fine(<35μm)	12	30	60	92

*C_u=d_{60}/d_{10} (coefficient of uniformity)

**C_c=$(d_{30})^2$/(d_{10}×d_{60})(coefficient of curvature)

2.2 High-stress permeability and consolidation apparatus

Fig. 2 presents the self-developed "High-stress Permeability and Consolidation Apparatus". The apparatus consists of a high-stress loading frame, a permeability cell, a control system and pressure sensors. The maximum axial consolidation load is 50 kN. The maximum pressure of 1.7 MPa can be supplied to the permeability cell by water exchange tanks. The maximum axial displacement is 100 mm. Permeability tests, consolidation tests and conjoined consolidation permeability tests can be performed in the apparatus. The maximum consolidation pressure can reach 15 MPa. The diameter of the specimen is 63.5 mm, and its height is 20 mm. The consolidation pressure is provided by the axial pressure p_1, and the water head is provided by the difference between the back pressure and the base pressure ($\Delta p = p_2 - p_3$). The prepared cutting ring samples are put into the permeability cell. The air expel hole is opened first to ensure that the permeability cell was filled with water.

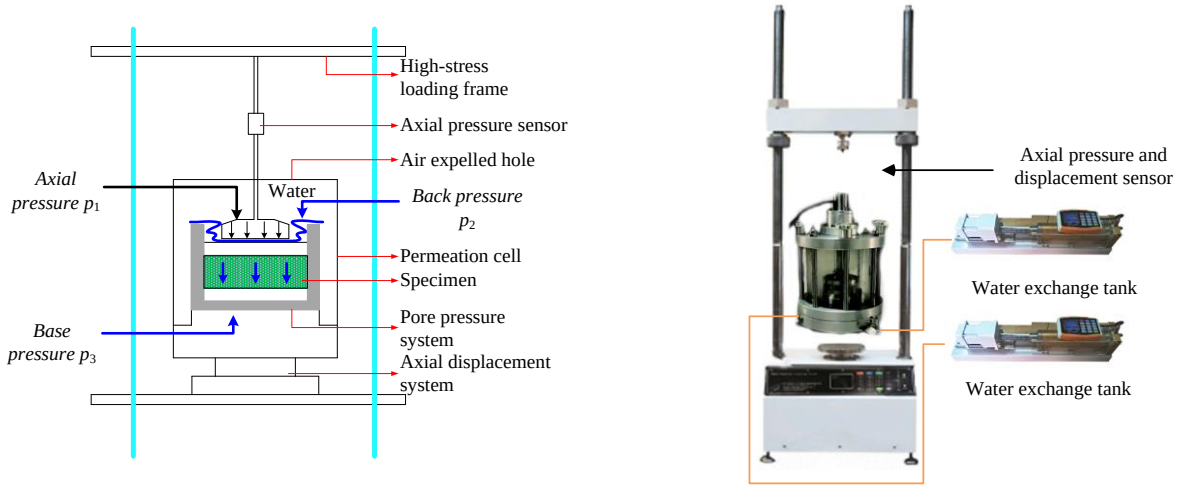

(a) Structural diagram (b) Real product

Fig. 2 High-stress permeability and consolidation apparatus

When the permeability cell is filled with distilled water the air expel hole is closed. The samples are compressed by the reaction force generated by the loading frame. The axial displacement is monitored by the displacement system in real time, and consolidation pressure is monitored by the axial pressure sensor in real time. The water in the permeability cell can be injected into the top of the sample and then flows into the water exchange tanks from the small hole at the bottom of the sample. The flow volume and pressure are displayed in real time. A structural diagram and the real product are shown in Fig. 2.

1) Consolidation tests: First, axial pressure p_1 and back pressure p_2 are applied together. p_1 was slightly larger than p_2, to ensure that there was a minor effective stress in the soil to prevent soil expansion. The difference between the axial pressure p_1 and the back pressure p_2 was kept constant, p_1 and p_2 were gradually increased to remove the air from the sample. When the bottom pore pressure increment Δu reached more than 93% of the back pressure increment Δp_2, the samples are considered as saturated. Then the consolidation tests were carried out by applying axial pressure p_1. Consolidation pressure is displayed on the computer terminal in real-time through the data collection system. 2) Permeability tests: The axial pressure p_1 was kept constant after each stage of consolidation. The valves on the seepage path were opened, and the water head was provided by the water exchange tank 1 and the water exchange tank 2. The principle of the permeability tests under the consolidation pressure are shown on the left in Fig. 2. 3) Conjoined consolidation permeability tests: After consolidation was completed at each stage of consolidation pressure ($p_1 - p_2$), $p_2 = p_3$, and the effective stress in the samples are equal to the consolidation pressure. p_1 was kept constant, p_2 and p_3 were set to conduct a permeability test to measure the hydraulic conductivity at this stage of consolidation. The consolidation tests were carried out after the samples were saturated, and the consolidation time was 24 h. The consolidation pressure was kept constant after the consolidation tests. The constant head permeability tests were carried out with the experiment duration was 1 h.

2.3 Test methods

Conjoined consolidation permeability tests were conducted under different consolidation pressures on samples S20, S02, S_75, S_35. All samples were prepared by the same procedure using the wet method because the sample structure is affected little by different sample preparation methods (wet, dry, or slurry) (Payan *et al.* 2016). To ensure uniformity, a small amount of distilled water was added to the tailings material in the containers (when the particle size is small, the added water is sprayed), and mixed in evenly. To ensure uniform mixing of the prepared tailings, the specimens were covered with plastic wrap 24 hours. The specimens were tamped in layers, and statically compacted with a compaction rate of 0.3 mm/min. The samples were finally shaped into a cylindrical sample with a diameter of 63.5 mm and a height of 20 mm, and a dry density of 1.6 g/cm^3.The specimens were then put into the container, covered with a porous stone and an upper-pressure plate. A pre-load was set of 0.01 kN to make sure the specimen is docked.

The consolidation pressures were set to 0.05 MPa, 0.1 MPa, 0.2 MPa, 0.4 MPa, 0.8 MPa, 1.2 MPa, 2 MPa, 3 MPa, 4 MPa, and 5 MPa, respectively. The loading rate ($\Delta p/p$) was designed to be 1 when the consolidation stress is less than 1 MPa. When the consolidation stress is greater than 1 MPa, the soil structure will be easily damaged in the load-increasing stage if the rate of 1 continues to be loaded. In order to get more data points and protect the sample structure during the high-pressure stage, the loading increment was set to 1 MPa. Tailings dams higher than 100 m are defined as high-stacked dams in some studies. When the height of the tailings sub-dam reaches 100 m, the mechanical response of deep tailings and surface tailings shows a large difference (Glotov *et al.* 2018). The tailings particle breakage under high pressure can not be negligible (Zhang *et al.* 2020), since it will result in a nonlinear increase in strength parameters. Nevertheless, so far, only a few mechanical tests of tailings under pressures above 2 MPa have been reported, and most of these studies have

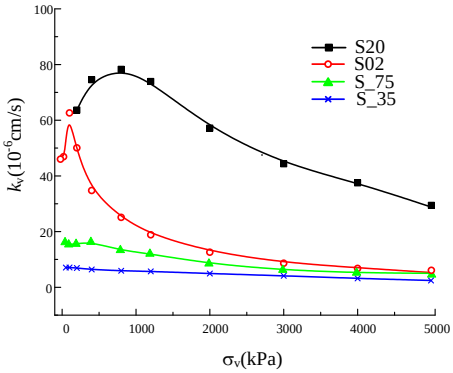

(a) k_v - σ_v

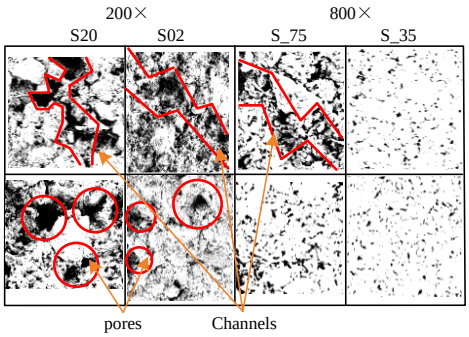

(b) SEM images

Fig. 3 Relationship between hydraulic conductivity (vertical axis) and consolidation pressure for four samples V: vertical section, H: horizontal section

focused on the strength parameters. The consolidation time at each stage is maintained for 24 h. Five permeability tests were carried out with different heights of water head after each stage of consolidation. The final hydraulic conductivity is the average of the five values. The water head is the difference between back pressure and base pressure Δp. The water inside the samples is in a downward and steady flow. The duration of each permeability test is 1 h.

3. Results and discussion

3.1 Permeability analysis

3.1.1 Seepage pattern

The hydraulic conductivities are shown in Fig. 3(a). With the increase of consolidation pressure, the hydraulic conductivity can be divided into three stages: (1) Unstable stage: When the consolidation pressure is low, the hydraulic conductivity changes irregularly due to the fact that the pores are loose and large. When the samples are subjected to consolidation pressure, the particles rearrange. The seepage channel then is easy to change. The unstable stage becomes shorter as the particle sizes decrease. (2) Rapid decrease stage: The hydraulic conductivity decreases rapidly as the consolidation pressure increases. This is because the sample is compacted as the consolidation pressure increases. The macropore seepage channel is fixed and shrinks with the increase of consolidation pressure. (3) Slow decrease stage: The hydraulic conductivity decreases slowly as the consolidation pressure increases further. When the particle size is large, the coarse particles contact each other, and the seepage channels remain basically unchanged. Fine particles were generated due to the breakage of coarse particles under high consolidation pressure. The change in hydraulic conductivity was slightly reduced by fine-particle blockage of the seepage channel. (Zhang *et al.* 2020). The three-stage properties of the hydraulic conductivity caused by the change of the seepage channel are called the channel flow. The hydraulic conductivity of channel flow is determined by a few large pore paths, while the hydraulic conductivity of scattered

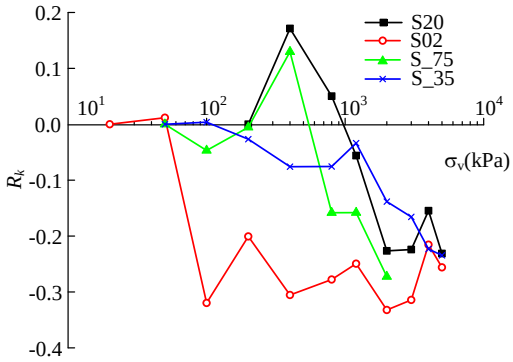

Fig. 4 Relationship between rate of change of hydraulic conductivity and consolidation pressure

flow is determined by many small pore paths. In the case of fine particles, the macropore seepage channel is closed due to the high viscosity of fine particles and the high consolidation pressure. The seepage pattern changes from channel flow to scattered flow (Erzsébet *et al.* 2019).

Fig. 3(b) shows SEM images that have been binarized after conjoined consolidation permeability tests with a maximum consolidation pressure of 5 MPa (for the binarization method see Ulusoy *et al.* 2003). The white areas represent solid particles, and the black areas represent pores. V represents the vertical section, and H represents the horizontal section. The images of S20 and S02 are magnified 200 times, and the images of S_75 and S_35 are magnified 800 times. The pores of S20 and S02 in the V section are obvious directional, The seepage channels are obvious (red lines) , and the pores are also obvious on the corresponding H section (red circles). The seepage channel is not obvious in S_75 and S_35. These observations verify that the seepage pattern in tailings with large particle size is channel flow, and the seepage pattern in tailings with small particle size is scattered flow.

To study the blocking effect of consolidation pressure on water in tailings of different particle sizes, parameter R_k is defined to characterize the degree of change in hydraulic conductivity:

$$R_k = \frac{k_n - k_{n-1}}{k_{n-1}} \tag{1}$$

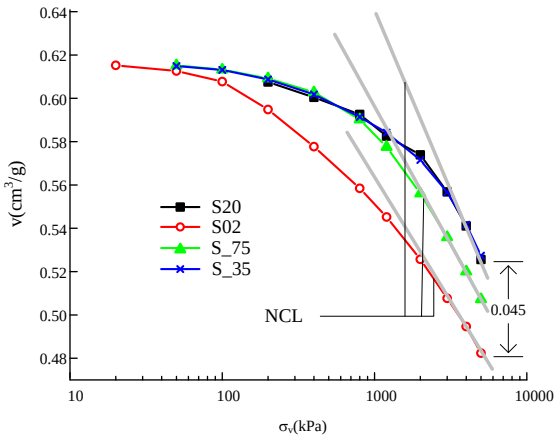

Fig. 5 One-dimensional compression characteristics of tailings samples

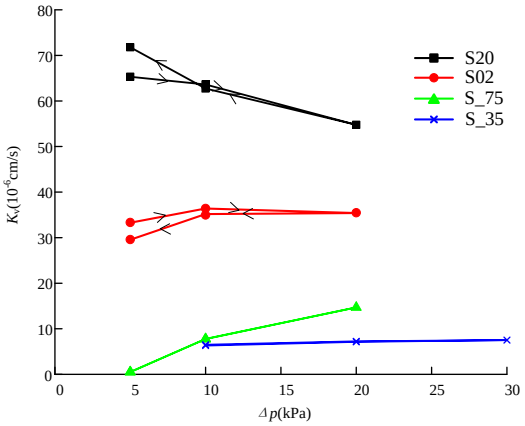

Fig. 6 Relationships between hydraulic conductivity and differential water head (400 kPa consolidation pressure)

where k_n is the hydraulic conductivity under a certain consolidation pressure, and k_{n-1} is the hydraulic conductivity under the previous consolidation pressure. When $n = 0$, $R_k = 0$, and the curves are shown in Fig. 4. It can be seen that after the consolidation stress reaches 400 kPa, different tailings samples tend to display similar change in hydraulic conductivity. When the consolidation pressure reaches 5 MPa, the R_k of different tailings samples is approximately equal to -0.23. High consolidation pressure can eliminate the influence of particle sizes on the change rate of the hydraulic conductivity of tailings.

3.1.2 Fabric analysis

Fig. 5 presents the v - σ_v curves for different particle sizes, where v is the specific volume (the reciprocal of the dry density, used to measure the volume change in compression tests) (Coop, 2015). When the initial specific volume is constant, the curves of S20 and S_35 are normalized to the same NCL (normal compression line), and the NCLs of S02 and S_75 are also normalized to a unified trend. However, a unique NCL cannot be obtained even when the consolidation stress reaches 5 MPa (a stress magnitude that is difficult to achieve on site). The difference in a specific volume at 5 MPa is 0.045, larger than the specific volume accuracy of approximately ± 0.02 calculated by different methods (Rocchi and Coop, 2014). Therefore, the one-dimensional non-convergent compression characteristics of tailings samples with different particle sizes are significant when the consolidation pressure is 5 MPa. NCLs tend to converge under higher consolidation pressures. This is consistent with the conclusion of Li *et al.* (2018). S02 showed the best compression performance, S20 and S_35 showed the worst compression performance.

3.1.3 Effect of water head on hydraulic conductivity

The hydraulic conductivities under different water heads are shown in Fig. 6. The hydraulic conductivities at 400 kPa consolidation pressure are taken as an example.

1) The hydraulic conductivities of S20 decrease with the increase of water head. 2) The hydraulic conductivities of S02 increase with the increase of water head. 3) The hydraulic conductivities of S_75 increase significantly with the increase of water head. When the water head is 5 kPa, the hydraulic conductivity is almost 0, which indicates S_75 has an obvious initial hydraulic gradient. 4) The hydraulic conductivities of S_35 are almost constant with the increase of water head. The hydraulic conductivity changes after the circulating water head show the hysteresis, which can be observed in both S20 and S02. Hysteresis is also found in the study of Gerard *et al.* (2019) of the permeability of saturated clay and hysteresis decreases with the increase of consolidation pressure. This hysteresis is different from hysteresis effects oberserved in hydraulic conductiviy versus suction and soil water characteristic curves related to unsaturated soils (Khoshghalb *et al.* 2014, Pasha *et al.* 2017). Fig. 6 shows that hysteresis is a unique phenomenon of channel flow (see section 3.1.1). After through higher water head, the specimens will undergo irreversible deformation. A detailed discussion is given later in this section.

Discussions on the change of hydraulic conductivity caused by increasing water head: The hydraulic conductivity of coarse-particle tailings decreases with the increases of the water head. When the content of fine particles increases, the hydraulic conductivity increases with the increase of the water head. The viscosity of the samples is enhanced due to the increase in the content of fine particles. The water in the tailings can be easily bound by the particles under a small head. The hydraulic conductivities of the ultra-fine sample S_35 remained constant, which may be related to the large pores caused by the similar particle size. Fig. 7 shows the XRD test results. Dexing tailings are composed mainly of quartz, illite, chlorite, albite and other minerals (including a small amount of calcite, dolomite, metallic minerals, etc.), and ω_q, ω_i, ω_c, ω_a and ω_o represent their mass fractions respectively. The coarse-particle tailings contain a higher mass fraction of quartz (non-clay minerals), and fine-particle tailings contain higher mass fractions of illite (clay minerals). From the perspective of mineral composition, the content of clay minerals of tailings increases as the content of fine tailings increases. The larger the fine particle content, the more obvious the increase of hydraulic conductivity with the increase of water head.

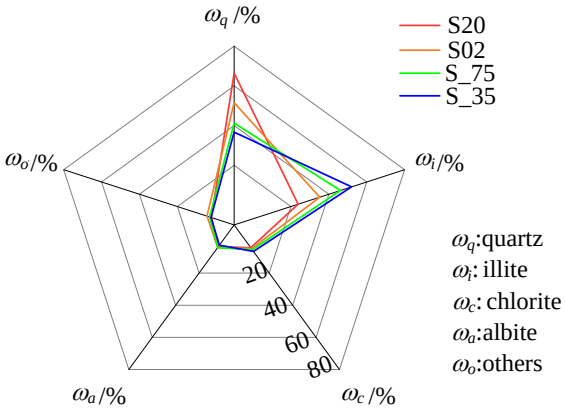

Fig. 7 The mass fraction of different minerals in tailings

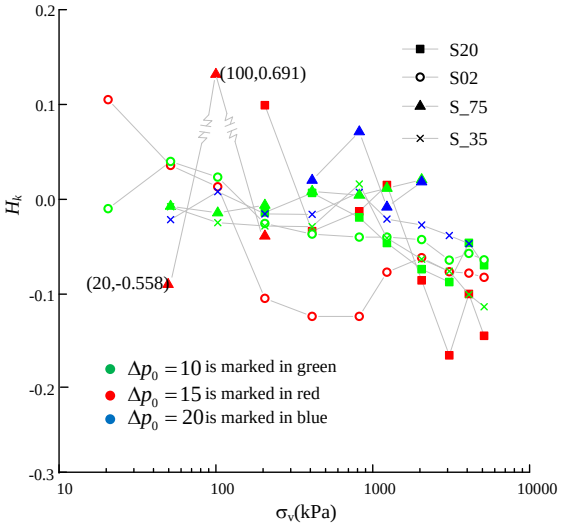

Fig. 8 Relationships between hysteresis coefficient H_k with consolidation pressure

Discussion on the effect of circulating water head on the change of hydraulic conductivity: S20 and S02 showed obvious hysteresis at a low water head of 5 kPa. The hydraulic conductivity of S20 at Δp = 5 kPa increases after the cyclic water head, and the hydraulic conductivity of S02 at Δp = 5 kPa decreased after the cyclic water head. The former is due to the irreversible widening of the seepage channel caused by the larger water head. The latter is due to the good compressibility of S02 (see Fig. 5), less irreversible deformation but greater disturbance (Blackwell *et al.* 1990).

In order to quantitatively analyze the influence of head on the hydraulic conductivity, the hysteresis coefficient H_k is defined.

$$H_k = \frac{k_v' - k_v}{k_v} \tag{2}$$

where k_v is the hydraulic conductivity under a certain water head, and k_v' is the hydraulic conductivity under the same water head after the cyclic water head. The parameter H_k eliminates the influence of the initial hydraulic conductivity and describes the influence of the hydraulic conductivity on

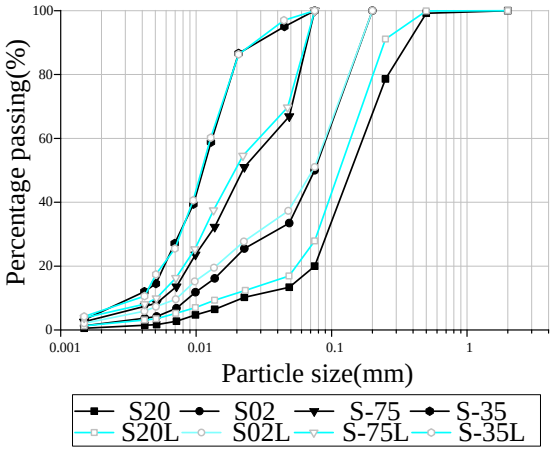

Fig. 9 Grading curves of all the samples

the head paths of different samples. $H_k > 0$ represents the anticlockwise head pressure paths (as shown for sample 20 in Fig. 6, the hydraulic conductivity increases after the cyclic water head), $H_k < 0$ represents the clockwise head pressure paths (as shown in S02 in Fig. 6, the hydraulic conductivity decreases after the cyclic water head). It can be seen from Fig. 8 that when the particle size is small, the tailings sample takes the clockwise osmotic pressure path.

When the initial head is 5 kPa, the data is obviously abnormal because Δp_0 = 5 kPa has not reached the initial hydraulic gradient of sample S_75; The smaller the initial head Δp_0, the farther the values of H_k are from the H_k = 0 axis. Increasing the initial head weakened the hysteresis. The strong water holding capacity of viscous tailings makes the samples compact and not easily disturbed (Gerard *et al.* 2019). H_k tends to decrease overall as the consolidation pressure increases to 5 MPa. The high consolidation pressure increases the compressibility of the sample, which reflects that the particle breakage under high consolidation pressure has an impact on the hydraulic conductivity.

3.2 Particle size analysis

S20 to S_35 are the samples for high-stress conjoined consolidation permeability tests, and S20L to S_35L are the samples after high-stress conjoined consolidation permeability tests. Fig. 9 presents the grading curves of the tailings. The C_u of S20 is higher than 5 and the C_c is between 1 and 3, so S20 is considered well-graded. Due to the lack of large particles, the gradation of S02, S_75, S_35 is getting worse than S20. S_75 and S_35 are considered as poorly graded (see Table 1). In the same figure, the results for S20L to S_35L after high-stress conjoined consolidation permeability tests are also given for comparison. Particle breakage is obvious.

Particle breakage is due to different particle size distribution and mineral composition, which affects the hydraulic conductivity of tailings, especially under high pressure (Zhang *et al.* 2020). Particle sizes (d_{10} - d_{90}) before consolidation are shown in Table 1. After the consolidation pressure reaches 5 MPa, the d_{10} changes from 0.023-0.003 mm to 0.016-0.003 mm, the d_{30} changes from 0.093-0.008 mm to 0.079 - 0.08 mm, the d_{50} changes from 0.141 - 0.011

mm to 0.113 - 0.011 mm, the d_{60} changes from 0.173 - 0.013 mm to 0.139 - 0.013 mm, and the d_{90} changes from 0.370 - 0.028 mm to 0.244 - 0.027 mm. Coarse particles are broken down more obviously than fine particles. The particle breakage decreases as the particle size decreases. The gradations of tailings samples are improved due to particle breakage as illustrated by the calculation of C_u and C_c.

4. Nonlinear permeability model of tailings

Taylor (1948) pointed out that the water permeability of clayey soil is different from that of sandy soil due to the plate-like morphology of the particles, and proposed the concept of effective void ratio. The compressibility and particle breakage of tailings are enhanced by the high consolidation pressure, which affects the hydraulic conductivity of tailings. In this section, the concepts of effective void ratio and breakage index are introduced to revise the hydraulic conductivity-void ratio relationship. The revised relationship will be applicable to the prediction of hydraulic conductivity of fine-particle tailings over a wide range of consolidation pressures.

4.1 Common hydraulic conductivity expressions fitting for each individual sample

Different hydraulic conductivity-void ratio expressions have been proposed by Terzaghi *et al.* (1996), Hazen (1911), Kozeny (1927), Amer and Awad (1974) and so on. The functional forms of these equations are roughly divided into three types: $k_v \propto e^2$, $k_v \propto \frac{e^2}{1+e}$ and $k_v \propto \frac{e^2}{1+e}$.

Fig. 10 shows the fitting results for three different type of functions. The slope K and the coefficient of determination R^2 are shown in Table 2. For individual samples, the fitting curves of S20 and S_35 show the best result, consistent with the results of experimental tests, followed by S02 and S_75. The applicability of the three function types becomes weaker as the particle size of the tailings decreases. However, when the D_{max} of the tailings is reduced to 35 μm, the functions are applicable. This may be due to the reduced irregularities of the clayey particles and pore size of the tailings with ultra-fine particles. The water film on the surface of the ultra-fine particles is firm due to its strong viscosity, which forms a structure similar to that of sandy particles. The expression $k_v \propto \frac{e^3}{1+e}$ is best suitable for tailings materials by comparing the coefficients of determination corresponding to the different functions.

The hydraulic conductivity-void ratio relationship of sandy soil is not applicable for clayey soil and plastic silty soil. The difference may due to the pore water viscosity and to the factors such as irregular particle and pore size, and a water film. The conductivity-void ratio equations of clayey soil are generally modified on the basis of the equations of sandy soil. Mesri and Olson (1971) proposed an equation on the basis of $k_v \propto e^2$:

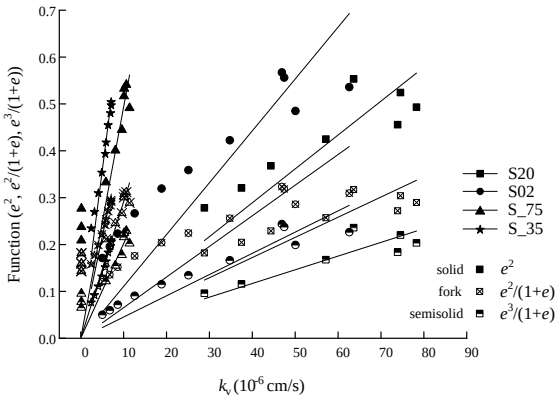

Fig. 10 Relationships between hydraulic conductivity and void ratios for three different functions

Table 2 Single sample fitting analysis of common sandy soil equation

Samples	S20		S02		S_75		S_35	
	K^*	R^2	K	R^2	K	R^2	K	R^2
e^2	0.007	0.555	0.011	0.489	0.049	0.218	0.071	0.927
$e^2/(1+e)$	0.004	0.180	0.007	0.005	0.029	1.149	0.043	0.742
$e^3/(1+e)$	0.003	0.746	0.005	0.801	0.020	0.440	0.028	0.983

*K is the slope of the fitting curves

$$k_v = Be^A \tag{3}$$

where A and B are the corresponding clayey soil permeability parameters. The equation (lg e – lg k_v) can also be expressed as:

$$\lg k_v = A\lg e + \lg B \tag{4}$$

Samarasinghe *et al.* (1982) proposed an equation on the basis of $k_v \propto \frac{e^2}{1+e}$ and $k_v \propto \frac{e^2}{1+e}$:

$$k_v = \frac{Ce^n}{1+e} \tag{5}$$

where C and n are parameters reflecting the soil properties. The equation (lg [k_v (1+e)] - lg e) can also be expressed as:

$$\lg[k_v(1+e)] = \lg C + n\lg e \tag{6}$$

Fig. 11 presents the test data regressed on the above two linear functions of clayey soil, Eq. (4) and Eq. (6). The results are summarized in Table 3.

lg e – lg k_v equation: The range of parameter A is 2.718 ~ 4.119. The range of parameter B is 3.629 ~ 10.40. The coefficient of determination R^2 is equal to 0.841 or higher, the fit is appropriate for single samples. However, the coefficient of determination R^2 is 0.237 for total samples. lg [k_v (1+e)] - lg e equation: The range of parameter n is 2.753 ~ 4.404. The range of parameter C is 4.784 ~ 12.922. The coefficient of determination R^2 is equal to 0.881 or higher.

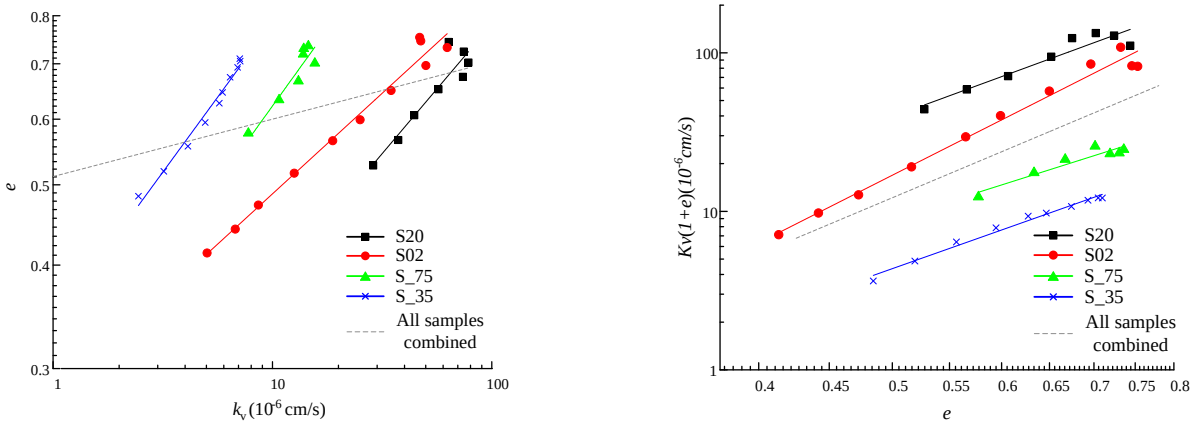

(a) lg e - lg k_v (b) lg [k_v (1+e)] - lg e

Fig. 11 Fitting results of two different clayey soil expressions for hydraulic conductivity-void ratio

Table 3 Samples fitting analysis of common clayey soil expressions for permeability as a function of void ratio

Samples	lg e – lg k_v			lg [k_v(1+e)] – lg e		
	A	B	R^2	n	C	R^2
S20	3.2	10.4	0.859	3.2	362.2	0.889
S02	4.1	9.8	0.979	4.4	357.9	0.983
S_75	2.7	4.1	0.841	2.8	72.7	0.881
S_35	2.8	3.6	0.978	3.1	36.6	0.984
All samples combined	0.08	3.5	0.237	2.7	73.5	0.289

The fit is better than that of the lg e – lg k_v model, and the lg [k_v (1+e)] - lg e model is preferable. However, the coefficient of determination R^2 is 0.289 for all samples combined.

The test data of the four groups of samples are concentrated on the same coordinate axis, and the linear fitting method is used for the total analysis. The coefficients of determination R^2 are 0.237 and 0.289. Therefore, the same kind of tailings with different D_{max} cannot be regarded as the same seepage medium. Various parameters (A, B, n, C) need to be calculated for each individual tailings medium. The application of common hydraulic conductivity-void ratio expressions in tailings dams is complicated due to the staggered middle layer and interlayers. In order to simplify the calculation, the liquid limit is introduced. Hydraulic conductivity of tailings materials of different particle sizes can be predicted by liquid limits w_l.

4.2 Revised expression fitting for total samples

4.2.1 Effective pores

The hydraulic conductivity of clayey soil and sandy soil is different due to the different influencing factors (Das, 2019). In this section, a unified equation is established to predict hydraulic conductivity for tailings samples of different particle sizes. An immobile water film is attached to the surface of fine-particle tailings. Pores that cannot participate in seepage are called ineffective pores. Ineffective pores in clayey soils account for almost 85% of the total pores (Quang *et al.* 2015).

The immobile water on the surface of clayey soils has low fluidity and high viscosity. Pore water pressure cannot be generated or transmitted in this immobile water. Therefore, the volume ratio of the pores occupied by the immobile water film on the particles is defined as the ineffective void ratio, denoted by e_0. The effective void ratio e_u is the difference between the total void ratio e and the ineffective void ratio e_0:

$$e_u = e - e_0 \tag{7}$$

By replacing the void ratio in the hydraulic conductivity-void ratio equation with the effective void ratio, the equation for different particle sizes can be unified. Combine Eq. (7) and Eq. (5):

$$k_v = \frac{C(e-e_0)^n}{1+e-e_0} \tag{8}$$

Eq. (8) is practical after giving the method for solving the ineffective void ratio e_0. Cui *et al.* (2010) pointed out that the state of water in the soil is determined by the position of water content relative to the liquid-plastic limit. As shown in Fig. 12, the content of hydroscopic water of clayey soil is between 0 ~ w_p, the content of film water is between w_p ~ w_l, and the total immobile water content is between 0 ~ $\alpha_0 w_l$ ($0<\alpha_0<1$). In other words, it is assumed that the plastic limit w_p of the sample is equivalent to the upper limit of hydroscopic water and the lower limit of film water. If the upper limit of immobile water is smaller than the liquid limit w_l of the soil, the immobile water content is equal to the liquid limit w_l multiplied by the reduction factor α_0. The effective void ratio e_u derived from the water film thickness is more consistent with the actual situation of compression tests. Compared with other expressions of e_u, the liquid limit w_l is easier to be obtained. α_0 is called the proportionality coefficient of immobile water to liquid limit w_l. For a certain type of clayey soil, α_0 can be approximated as a constant. For Dexing tailings, α_0 is obtained by the results of experimental tests, and $\alpha_0 = 0.9$ in this paper. So, it can be deduced as follows:

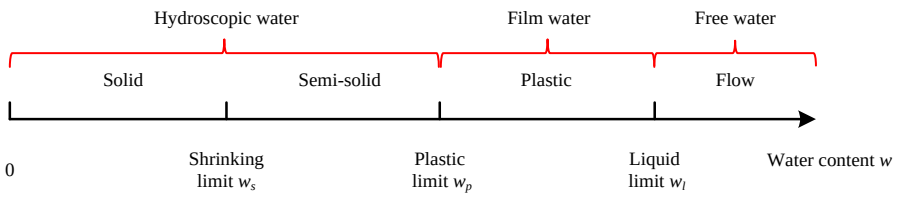

Fig. 12 Hypothetical physical state of clayey soil and water content

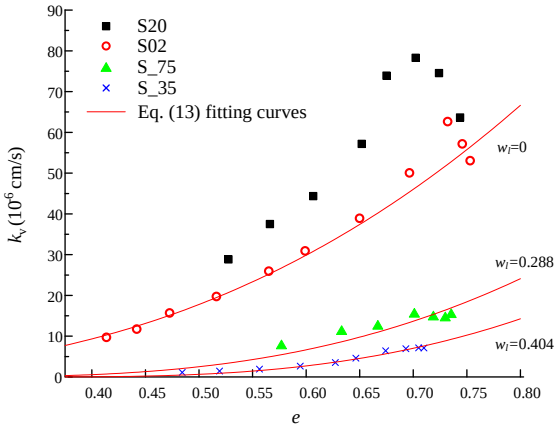

Fig. 13 Fitting curves of hydraulic conductivity considering effective void ratio

The immobile water content corresponding to the ineffective void ratio is

$$w_a = \frac{m_{aw}}{m_s} = \alpha_0 w_l \tag{9}$$

where m_{aw} is the mass of immobile water, and its unit is g. m_s is the mass of soil particles, and its unit is g. So,

$$m_{aw} = m_s w_a = \alpha_0 \rho_s V_s w_l \tag{10}$$

where ρ_s is the density of soil particles, and its unit is g/cm^3. V_s is the total volume of soil particles, and its unit is cm^3. The ineffective void ratio is

$$e_0 = \frac{V_{aw}}{V_s} = \frac{m_{aw}/\rho_w}{V_s} = \frac{\alpha_0 \rho_s V_s w_l}{V_s \rho_w} = \alpha_0 \frac{\rho_s}{\rho_w} w_l = \alpha_0 G_s w_l \tag{11}$$

where V_{aw} is the total volume of immobile water, and its unit is cm^3. ρ_w is the density of water, and its unit is g/cm^3. G_s is the relative density, and it is a non-dimensional parameter. Thus, the effective void ratio is

$$e_u = e - e_0 = e - \alpha_0 G_s w_l \tag{12}$$

Putting Eq. (12) back into Eq. (8) gives

$$k_v = \frac{C(e - \alpha_0 G_s w_l)^n}{1 + e - \alpha_0 G_s w_l} \tag{13}$$

The fitting curves and experimental test results are shown in Fig. 13 (red solid lines). There is no liquid limit in S20 and S02 due to they being non-clayey soil, set w_l = 0, and other parameter values are given in Table 1. The tailings parameter n is 3.2 and C is 245.

After the concept of effective void ratio e_u was introduced, the hydraulic conductivity-void ratio equation of clayey tailings and non-clayey tailings has been unified, and the fitting curves are consistent with the results of experimental tests. The difference between the actual points and the calculated points is not more than one order of magnitude. Since there is no liquid limit for non-clayey tailings, the effective void ratio revised equation cannot give the curves of S20 and S02, respectively.

4.2.2 Particle breakage

The particle breakage index B_r proposed by Hardin (1985) is based on the change of the entire particle size distribution. Hardin (1985) limits the minimum threshold of particle size to 0.074 mm. Different thresholds have been proposed by different scholars (Daouadji *et al.* 2012, McDowell *et al.* 1996). Under high consolidation pressure, particle breakage still occurs when the particle size is less than 0.074 mm (Shahnazari and Rezvani 2013). Einav (2007) proposed a particle size accumulation curve to express the breaking rate of tailings particles under high stress. The particle size distribution before the test is defined as P_0, the particle size distribution after the test is defined as P_c, and the particle size distribution after the ultimate pressure is defined as P_u. Then the particle breakage index is:

$$B_r = (F_c - F_0)/(F_u - F_0) \tag{14}$$

$$F_0 = \int_{d_{min}}^{d_{max}} P_0 \, \mathrm{d}(d) \tag{15}$$

$$F_c = \int_{d_{min}}^{d_{max}} P_c \, \mathrm{d}(d) \tag{16}$$

$$F_u = \int_{d_{min}}^{d_{max}} P_u \, \mathrm{d}(d) \tag{17}$$

where d_{min} and d_{max} are the minimum particle size and the maximum particle size respectively. The particle size distribution after the ultimate pressure P_u is not easy to obtain in tests. However, P_u can be obtained by inverse calculation of F_c (See Daouadji *et al.* 2012). The breakage index ranges from 0 to 1. B_r = 0 means that the tailings particles are not broken, and B_r = 1 means that all the particles are broken. Through calculation, the breakage index B_r of S20, S02, S_75 and S_35 under 5 MPa.

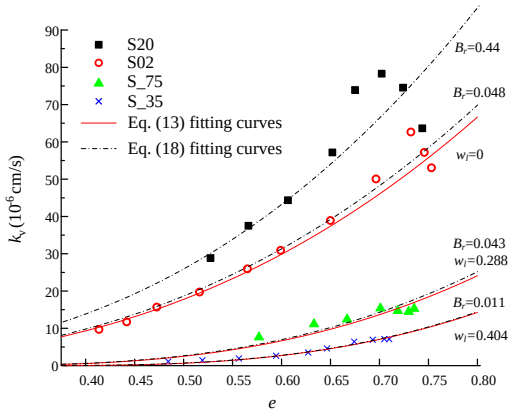

Fig. 14 Fitting curves of hydraulic conductivity after introducing the concept of effective void ratio e_0 and breakage index B_r

consolidation pressure are 0.44, 0.048, 0.043 and 0.011, respectively. Particle breakage under high consolidation pressure has a more significant impact on coarse-particle tailings. When considering the impact of particle sizes on water permeability properties, the breakage rate B_r is a factor that cannot be ignored.

In the hydraulic conductivity-void ratio equation, it is generally considered that there is a characteristic particle size d_{10}, where $k_v \propto d_{10}^2$ (e.g., Terzaghi *et al.* 1996, Hazen 1911). The essence of particle breakage is the conversion of energy, and the particle breakage rate is related to the area of the particles (i.e. $B_r \propto d_{10}^2$). Combined with Eq. (13), the hydraulic conductivity-void ratio relationship considering the breakage rate B_r and effective void ratio e_0 can be expressed as:

$$k_v = \frac{C(e-\alpha_0 G_s w_l)^n}{1+e-\alpha_0 G_s w_l}(1+B_r) \tag{18}$$

The modified fitting curves are shown in Fig. 14 (black dashed lines). The tailings parameters are still 3.2 for n and 245 for C. It can be seen that the model modified by the breakage index provides a good prediction of the hydraulic conductivity of S20 and S02, and successfully improved the shortcoming for non-clayey soil without liquid limit parameters. Fitting curves of the four tailings samples with different particle sizes are consistent with the results of experimental tests and are represented well by Eq. (18).

5. Conclusions

- The hydraulic conductivity of coarse-particle tailings presents an obvious three-stage change with the increase of consolidation pressure, which is due to the seepage pattern of coarse-particle tailings as channel seepage. The three-stage characteristic is not obvious with the increase of the fine particle content, and the seepage pattern of the sample is transformed from channel flow to scattered flow. The hydraulic conductivity change rate R_k of tailings samples with different particle sizes converges with the increase of consolidation pressure. High consolidation pressure can eliminate the influence of particle sizes on the change rate R_k of the hydraulic conductivity of tailings.

- The hydraulic conductivity of coarse-particle tailings decreases with the increase of water head. The hydraulic conductivity of fine-particle tailings increases with the increase of water head, and the hydraulic conductivity of ultra-fine particle tailings basically remains constant with the increase of water head. Increasing the initial head and decreasing particle size weakened the hysteresis. The hysteresis is caused by irreversible deformation of the seepage channels and disturbance of samples. The hysteresis coefficient of hydraulic conductivity generally decreases with the increase of consolidation pressure, reflecting the impact of particle breakage on hydraulic conductivity under high consolidation pressure.

- Based on the particle size distribution, the properties of tailings with different sizes are analyzed. Decreasing particle size increases the proportion of clayey mineral components and particle breakage. The particle breakage induces a certain improvement effect on the tailings grading.

- The fitting parameters of each layer need to be obtained separately when material partitioning is used to predict hydraulic conductivity in the tailings dam. In order to simplify the prediction method, the concepts of effective void ratio and breakage index were introduced to modify the hydraulic conductivity equation. The revised equation is applied for the prediction of hydraulic conductivity of tailings with different particle sizes under a wide range of consolidation pressure. The compression and consolidation characteristics of tailings with different material region are important. Further research is worth conducting to high-stress consolidation tests.

Data availability statement

Some or all data or models generated or used during the study are available from the corresponding author by request.

Acknowledgments

The research described in this paper was financially supported by the National Key Research and Development Program of China (Grant NO. 2017YFC0804601). National Natural Science Foundation of China (No. 51741410). The authors are sincerely grateful to Prof. Jaak J Daemen, Mackay School of Earth Sciences and Engineering, University of Nevada, for his thoughtful proofreading of this paper.

References

Amer, A.M. and Awad, A.A. (1974), “Permeability of cohesionless

soils", *J. Geotech. Geoenviron. Eng.*, **100**(12), 1309-1316. https://doi.org/10.1061/AJGEB6.0000134.
ASTM (2017), Standard Test Methods for Liquid Limit, Plastic Limit, and Plasticity Index of Soils, ASTM International, West Conshohocken, Pennsylvania, U.S.A.
Bernabé, Y., Li, M. and Maineult, A. (2010), "Permeability and pore connectivity: A new model based on network simulations", *J. Geophys. Res. Solid Earth*, **115**(1), 46-52. https://doi.org/10.1029/2010JB007444.
Blackwell, P.S., Ringrose-Voase, A.J. and Jayawardane, N.S. (1990), "The use of air-filled porosity and intrinsic permeability to air to characterize structure of macropore space and saturated hydraulic conductivity of clay soils", *J. Soil Sci.*, **41** (2), 215-228. https://doi.org/10.1111/j.1365-2389.1990.tb00058.x.
Carman, P.C. (1937), "Fluid flow through a granular bed", *Trans. Inst. Chem. Eng.*, **15**, 150-156.
Coop, M.R. (2015), "Limitations of a critical state framework applied to the behavior of natural and 'transitional' soils", *Proceedings of the 6th International Symposium on Deformation Characteristics of Geomaterials*, Buenos Aires, Argentina, November.
Courtney, D., Sumi, S. and Deborah, J.R. (2017), "Geotechnical properties of polymer-amended tailings solvent recovery unit (TSRU) oil sands tailings", *Can. Geotech. J.*, **54**(9), 1331-139. https://doi.org/10.1139/cgj-2016-0028.
Cui, D.S., Xiang, W., Cao, L.J. and Liu, Q.B. (2010), "Experimental study on reducing thickness of adsorbed water layer for red clay", *Chin. J. Geotech. Eng.*, **32**(6), 944-949. https://doi.org/10.4081/bam.2014.1.21.
Das, B.M. (2019), *Advanced Soil Mechanics*, CRC Press.
Daouadji, A., Hicher, P.Y. and Rahma, A. (2001), "An elastoplastic model for granular materials taking into account grain breakage", *Eur. J. Mech. A. Solids*, **20**(1), 113-137. https://doi.org/10.1016/S0997-7538(00)01130-X.
Einav, I. (2007), "Breakage mechanics-part I: Theory", *J. Mech. Phys. Sol.*, **55**(6), 1274-1297. https://doi.org/10.1016/j.jmps.2006.11.003.
Erzsébet, T., Tamás, G. and Weiszburg, J.T. (2010), "Submicroscopic accessory minerals overprinting clay mineral REE patterns (celadonite-glauconite group examples)", *Chem. Geol.*, **269**(3-4), 312-328. https://doi.org/10.1016/j.chemgeo.2009.10.006.
Gerard, P., Harrington, J., Charlier, R. and Collin, F., (2014), "Modelling of localized gas preferential pathways in claystone", *Int. J. Rock Mech. Min. Sci.*, **67**, 104-114. https://doi.org/10.1016/j.ijrmms.2014.01.009.
Gomes, L.E.D.O., Correa, L.B., Sá, F., Neto, R.R. and Bernardino, A.F. (2017), "The impacts of the Samarco mine tailing spill on the Rio Doce estuary, Eastern Brazil", *Mar. Pollut. Bull.*, **120**(1-2), 28-36. https://doi.org/10.1016/j.marpolbul.2017.04.056.
Glotov, V.E., Chlachula, J., Glotova, L.P. and Little, E. (2018), "Causes and environmental impact of the gold-tailings dam failure at Karamken, the Russian Far East", *Eng. Geol.*, **245**, 236-247. https://doi.org/10.1016/j.marpolbul.2017.04.056.
Hardin, B.O. (1985), "Crushing of soil particles", *J. Geotech. Eng.*, **111**(10), 1177-1192. https://doi.org/10.1016/0148-9062(86)91168-X.
Hazen, A. (1911), "Discussion of dams on sand foundations", *Trans. Am. Civ. Eng.*, **73**(3), 190-207.
Hilfer, R. (1991), "Geometric and dielectric characterization of porous media", *Phys. Rev. B*, **44**(1), 60-75. https://doi.org/10.1103/PhysRevB.44.60.
Horpibulsuk, S., Yangsukkaseam, N., Chinkulkijniwat, A. and Du, Y.J. (2011), "Compressibility and permeability of Bangkok clay compared with kaolinite and bentonite", *Appl. Clay Sci.*, **52**(1-2), 150-159. https://doi.org/10.1016/j.clay.2011.02.014.
James, M., Aubertin, M., Wijewickreme, D. and Wilson, G.W. (2011), "A laboratory investigation of the dynamic properties of tailings", *Can. Geotech. J.*, **48**(11), 1587-1600. https://doi.org/10.1139/t11-060.
Jang, J., Narsilio, G.A. and Santamarina, J.C. (2011), "Hydraulic conductivity in spatially varying media - a pore-scale investigation", *Geophys. J. Int.*, **184**(3), 1167-1179. https://doi.org/10.1111/j.1365-246X.2010.04893.x.
Khoshghalb, A., Russell, A.R. and Yang, H. (2014), "Fractal-based estimation of hydraulic conductivity from soil-water characteristic curves considering hysteresis", *Géotech. Lett.*, **4**(1-3), 1-10. https://doi.org/10.1680/geolett.13.00071.
Kim, B.S., Kato, S. and Park, S.W. (2019), "Experimental approach to estimate strength for compacted geomaterials at low confining pressure", *Geomech. Eng.*, **18**(5), 459-469. https://doi.org/10.12989/gae.2019.18.5.459.
Kozeny, J. (1927), "über kapillare Leitung des Wassers im Boden", *Sitz. Der Wien.*, **136**, 271-306.
Lambe, T.W. and Whitman, R.V. (1969), *Soil Mechanics*, John Wiley and Sons, Inc., New York, U.S.A., 281-294.
Li, W., Coop, M.R., Senetakis, K. and Schnaid, F. (2018), "The mechanics of a silt-sized gold tailing", *Eng. Geol.*, **241**, 97-108. https://doi.org/10.1016/j.enggeo.2018.05.014.
McDowell, G.R., Bolton, M.D. and Robertson, D. (1996), "The fractal crushing of granular materials", *J. Mech. Phys. Soil.*, **44**(12), 2079-2101. https://doi.org/10.1016/S0022-5096(96)00058-0.
Mesri, G. and Olson, R.E. (1971), "Mechanisms controlling the permeability of clays", *Clay. Clay. Miner.*, **19**(3), 151-158. https://doi.org/10.1346/CCMN.1971.0190303.
Pasha, A.Y., Khoshghalb, A., Khalili, N. (2017), "Hysteretic model for the evolution of water retention curve with void ratio", *J. Eng. Mech.*, **143**(7), 04017030. https://doi.org/10.1061/(ASCE)EM.1943-7889.0001238.
Payan, M., Khoshghalb, A., Senetakis, K., Khalili, N. (2016), "Effect of particle shape and validity of Gmax models for sand: A critical review and a new expression", *Comput. Geotech.*, **72**, 28-41. https://doi.org/10.1016/j.compgeo.2015.11.003.
Quang, N.D. and Chai, J.C. (2015), "Permeability of lime- and cement-treated clayey soils", *Can. Geotech. J.*, **52**(9), 1-7. https://doi.org/10.1139/cgj-2014-0134.
Robert, M.K. (2000), "Emerging and future development of selected geosynthetic applications", *J. Geotech. Geoenviron Eng.*, **126**(4), 293-306. https://doi.org/10.1061/(ASCE)1090-0241(2000)126:4(293).
Rocchi, I. and Coop, M.R. (2014), "Experimental accuracy of the initial specific volume", *Geotech. Test. J.*, **37**(1), 169-175. https://doi.org/10.1520/GTJ20130047.
Samarasinghe, A.M., Huang, Y.H. and Drnevich, V.P. (1982), "Permeability and consolidation of normally consolidated soils", *J. Geotech. Eng. Div.*, **108**(6), 835-850. https://doi.org/10.1016/0022-1694(82)90165-2.
Shahnazari, H. and Rezvani, R. (2013), "Effective parameters for the particle breakage of calcareous sands: An experimental study", *Eng. Geol.*, **159**, 98-105. https://doi.org/10.1016/j.enggeo.2013.03.005.
Tavenas, F., Jean, P., Leblond, P. and Lerouell, S. (1983), "The permeability of natural soft soil clays, part II: Permeability characteristics", *Can. Geotech. J.*, **20**(4), 645-660. https://doi.org/10.1139/t83-073.
Taylor, D.W. (1948), *Fundamentals of Soil Mechanics*, John Wiley and Sons, Inc., New York, U.S.A., 97-123.
Terzaghi, K., Peck, R.B. and Mesri, G. (1996), *Soil Mechanics in Engineering Practice*, John Wiley & Sons.
Ulusoy, U., Yekeler, M. and Hiçyılmaz, C. (2003), "Determination of the shape, morphological and wettability properties of quartz and their correlations", *Miner. Eng.*, **16**(10), 951-964. https://doi.org/10.1016/j.mineng.2003.07.002.

Wang, G.J., Sen, T., Bin, H., Kong, X.Y. and Chen, J. (2020), "An experimental study on tailings deposition characteristics and variation of tailings dam saturation line", *Geomech*. *Eng*., **23**(1), 85-92. https://doi.org/10.12989/gae.2020.23.1.085.

Zhang, C., Chen, Q., Pan, Z. and Ma, C. (2020), "Mechanical behavior and particle breakage of tailings under high confining pressure", *Eng*. *Geol*., **265**, 105419. https://doi.org/10.1016/j.enggeo.2019.105419.

CC